

Efficient One-Step Conversion of a Low-Grade Vegetable Oil to Biodiesel over a Zinc Carboxylate Metal–Organic Framework

Valentino Bervia Lunardi,[†] Fransiska Gunawan,[†] Felycia Edi Soetaredjo, Shella Permatasari Santoso,* Chun-Hu Chen, Maria Yuliana, Alfin Kurniawan, Jenni Lie, Artik Elisa Angkawijaya, and Suryadi Ismadji*



Cite This: *ACS Omega* 2021, 6, 1834–1845



Read Online

ACCESS |



Metrics & More

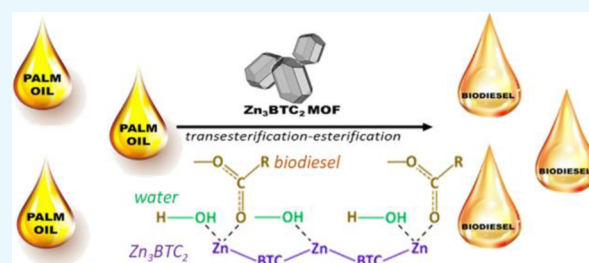


Article Recommendations



Supporting Information

ABSTRACT: In this study, a metal–organic framework, namely, $Zn_3(BTC)_2$ (BTC = 1,3,5-benzenetricarboxylic acid), was solvothermally synthesized and employed as a catalyst for biodiesel production from degummed vegetable oil via a one-step transesterification and esterification reaction. The resulting $Zn_3(BTC)_2$ particles exhibit a well-defined triclinic structure with an average size of about 1.2 μm , high specific surface area of 1176 m^2/g , and thermal stability up to 300 $^\circ\text{C}$. The response surface methodology–Box–Behnken design (RSM–BBD) was employed to identify the optimal reaction conditions and to model the biodiesel yield in relation to three important parameters, namely, the methanol/oil molar ratio (4:1–8:1), temperature (45–65 $^\circ\text{C}$), and time (1.5–4.5 h). Under the optimized reaction conditions (i.e., 6:1 methanol/oil molar ratio, 65 $^\circ\text{C}$, 4.5 h), the maximum biodiesel yield reached 89.89% in a 1 wt % catalyst, which agreed very well with the quadratic polynomial model's prediction (89.96%). The intrinsic catalytic activity of $Zn_3(BTC)_2$, expressed as the turnover frequency, was found to be superior to that of other MOF catalysts applied in the transesterification and esterification reactions. The reusability study showed that the as-synthesized $Zn_3(BTC)_2$ catalyst exhibited good stability upon three consecutive reuses without a noticeable decrease in the methyl ester yield ($\sim 4\%$) and any appreciable metal leaching ($< 5\%$). Furthermore, a preliminary techno-economic analysis showed that the total direct operating cost for the kilogram-scale production of $Zn_3(BTC)_2$ is estimated to be US\$50, which may sound economically attractive.



1. INTRODUCTION

Biomass-derived energy sources are considered a promising solution to the global energy crisis resulting from the overconsumption and continuous depletion of finite fossil fuel reserves. In this context, biodiesel has drawn wide attention as a green and sustainable alternative to petroleum-derived diesel fuels owing to its similar properties, inherent lubricity, and lower net emissions of carbon monoxide (CO), particulate matter (PM), and unburned hydrocarbons. The high oxygen content of biodiesel can also contribute to reducing soot formation, leading subsequently to a cleaner and more efficient combustion.^{1,2} Apart from the less polluting exhaust emissions, the rapid escalation in biodiesel consumption and production worldwide may build up the atmospheric concentrations of CO₂ and other greenhouse gases. Plant cultivation in biodiesel feedstocks can help establish a sustainable and net-zero carbon-neutral cycle through the Calvin–Benson–Bassham photosynthetic cycle.³ Moreover, plant biomass utilization provides additional benefits such as renewability, nontoxicity, and biodegradability.^{4–6} While such an energy crop plantation scenario presents a promising opportunity for the sustainability of biodiesel production, one can reasonably expect adverse

socioeconomic and biodiversity impacts as a result of the considerable land use and land-use changes. In addition, the use of edible crops for biodiesel feedstock may raise a contentious issue of food vs fuel, specifically in underdeveloped and developing regions. Therefore, the biodiesel industries' policy measures and implementation are vital in tackling the above issues and achieving a wider social acceptance.

While research and development of biodiesel have been continuously pursued during the last two decades, the economic viability of the process remains a significant barrier to widespread commercialization.⁷ In this context, the utilization of nonedible low-cost feedstock oils and the development of highly active, economic, and easily recyclable catalysts represent two major strategies to make the biodiesel production process more economically attractive. The latter strategy has become the main focus of the biodiesel research

Received: August 10, 2020

Accepted: January 4, 2021

Published: January 14, 2021



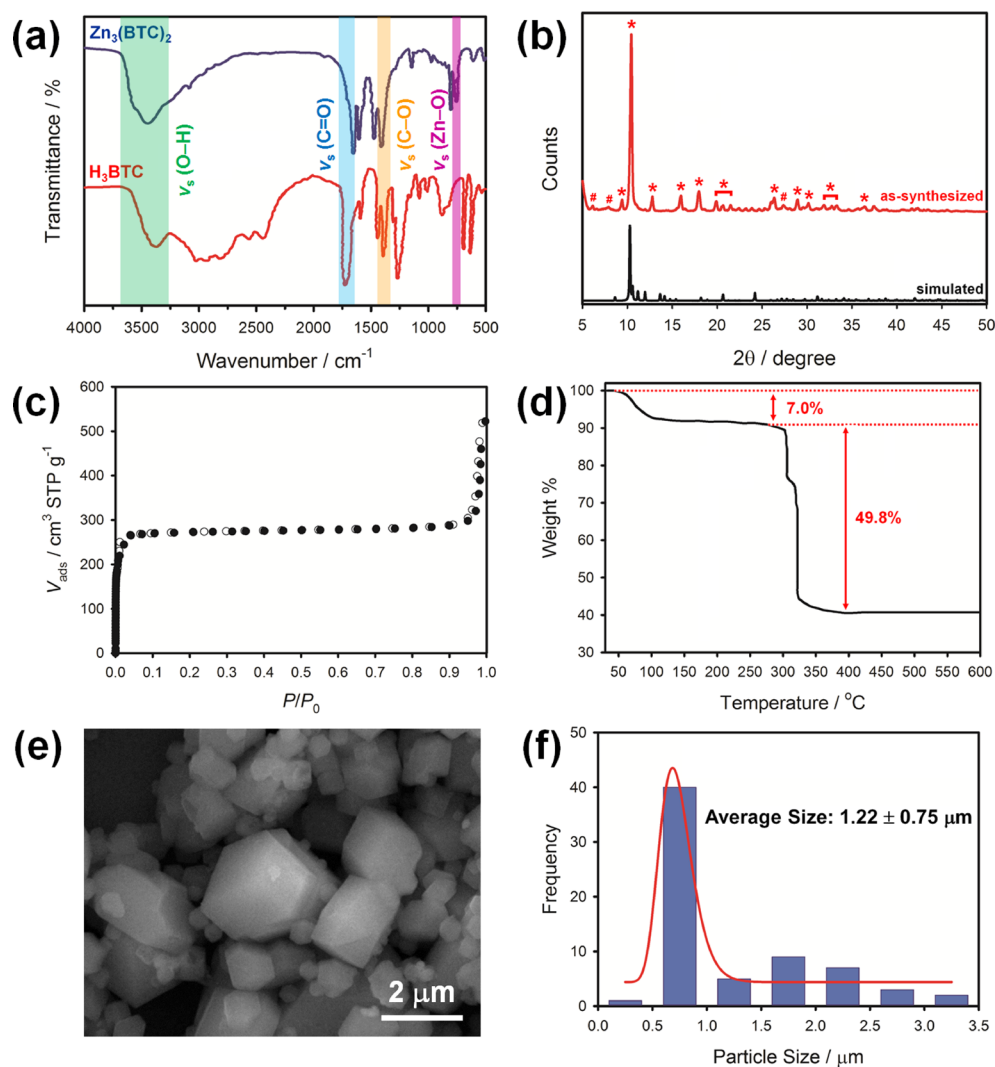


Figure 1. Characterizations of the $\text{Zn}_3(\text{BTC})_2$. (a) FTIR spectra of the H_3BTC linker and as-synthesized $\text{Zn}_3(\text{BTC})_2$. (b) Powder XRD patterns of the as-synthesized $\text{Zn}_3(\text{BTC})_2$ along with the simulated diffraction pattern from CCDC-664416. The Bragg reflections denoted with asterisks (*) and octothorpe (#) indicate the crystal lattice of $\text{Zn}_3(\text{BTC})_2$ and impurity phases, respectively. (c) Nitrogen adsorption–desorption isotherms of $\text{Zn}_3(\text{BTC})_2$ at 77 K. The solid and hollow circles represent the adsorption and desorption branches of the isotherm, respectively. (d) Thermogravimetric weight loss of $\text{Zn}_3(\text{BTC})_2$ recorded under a N_2 atmosphere. (e) SEM images of polydisperse $\text{Zn}_3(\text{BTC})_2$ particles and (f) the particle size distribution histogram obtained by measuring more than 60 randomly selected particles on the SEM image using the Fiji-ImageJ software. The red line in the histogram represents the best-fit log-normal distribution ($R^2 = 0.96$) obtained using the SigmaPlot software.

community toward improving product yield, which in turn reduces the total manufacturing costs. Homogeneous catalytic systems based on alkali metal hydroxides (e.g., NaOH or KOH) or related alkoxides suffer from the intricate and costly separation and recycling of the catalyst after the reaction. Moreover, the practical utility of homogeneous alkaline catalysts is complicated by the stringent demand for expensive refined lipid feedstocks in the process. On the other hand, heterogeneous catalysts allow for the easy recovery and reuse for multiple reaction cycles, as well as possess a comparatively high activity to homogeneous catalysts. Various solid acid and base catalysts with tunable structural and surface functionalities have been extensively developed, and many of them show promising activity for improving the biodiesel production yield.^{4,8} Heterogeneous solid base catalysts generally afford faster reaction rates and therefore higher biodiesel yields compared with the acid counterparts under milder reaction conditions. However, they are sensitive to free fatty acids

(FFAs; max. 2 wt %) and water content (<0.06 wt % or 600 ppm tolerable level) in the starting feedstock,^{9–11} which can promote saponification and hydrolysis side reactions and decrease both the catalyst activity and the ester yield. Hence, the solid acid catalysts remain the preferred choice when dealing with low-quality or nonedible vegetable oils containing significant quantities of FFAs and water.

Metal–organic frameworks (MOFs) have emerged as an attractive and versatile porous crystalline material in the realm of heterogeneous catalysis, thanks to their unprecedented attributes, such as exceptionally high internal surface areas, tailorable nanoscale porosity, enormous structural and chemical diversity, good thermal stability, and modular synthetic design.¹² The open metal sites (OMS; also referred to as coordinatively unsaturated metal centers) in the MOF structure are known to behave as the adsorption and Lewis acidic sites, thus playing a central role in modulating the catalytic activity and selectivity for various reactions. To date,

numerous studies have demonstrated the outstanding performance of MOF catalysts to achieve both high conversion efficiency and selectivity in a variety of industrially relevant reactions; however, less attention has been paid to the transesterification and esterification reactions. With respect to the biodiesel production, only a few types of MOFs have been investigated, such as iron and copper benzenetricarboxylate (Fe-BTC and Cu-BTC), MIL-53(Fe), UiO-66, and Cr(III) and Co(II) terephthalate.^{7,8,13,14} While these MOF catalysts can afford fatty acid alkyl esters in good to excellent yields (85–98%), the conversion is accomplished by either esterification using well-defined fatty acid substrates (e.g., oleic acid)^{13,14} or a two-step trans/esterification of pre-esterified oil,⁷ while the model reaction featuring a one-step trans/esterification remains unexplored.

In this study, the catalytic performance of a three-dimensional (3D) Zn(II)-based carboxylate MOF (hereafter denoted as $Zn_3(BTC)_2$) is examined for direct conversion of degummed palm oil (DPO) to biodiesel via the simultaneous transesterification and esterification in methanol. The one-step process of transesterification and esterification provides an economic advantage and improves the efficiency of biodiesel production.¹⁵ Based on the intensive review of available literature, the $Zn_3(BTC)_2$ MOF has been applied to various organic transformation reactions, such as the alkylation of toluene with benzyl bromide, cycloaddition of carbon dioxide to cyclic carbonates, synthesis of benzimidazole derivatives, and Knoevenagel condensation.^{16–19} To the best of our knowledge, this study is the first to report the catalytic activity of $Zn_3(BTC)_2$ for the transesterification and esterification of a low-grade vegetable oil (DPO) to produce fatty acid methyl esters (FAMEs) or biodiesel. The second objective of this study is to pinpoint the optimal conditions for maximizing the conversion efficiency of $Zn_3(BTC)_2$ -catalyzed biodiesel production by the response surface methodology (RSM). The preliminary cost analysis of the MOF synthesis on a kilogram scale is also provided to assess the economic potential of $Zn_3(BTC)_2$ as an efficient and reusable solid acid catalyst.

2. RESULTS AND DISCUSSION

2.1. Structure and Characterization of the $Zn_3(BTC)_2$ Catalyst. The 3D porous $Zn_3(BTC)_2$ MOF is constructed from the coordination interaction between the tritopic linker H_3BTC and Zn^{2+} ions in a multidentate fashion.²⁰ In the formation of $Zn_3(BTC)_2$, the H_3BTC linkers are fully deprotonated to form a negatively charged BTC^{3-} species. The polar aprotic DMF molecules act as a mobile phase that assists the interactions between Zn^{2+} ions and the deprotonated BTC^{3-} ligands. Meanwhile, the Zn metal centers are six-coordinated with two carboxyl oxygen atoms in two independent BTC^{3-} ligands and four oxygen atoms belonging to water molecules to form an octahedral coordination geometry. The resultant octahedral coordination environment with an extensive hydrogen bonding among water eventually leads to the formation of a stable crystalline framework between the carboxylate groups of BTC^{3-} and Zn^{2+} ion.^{20,21}

The formation of $Zn_3(BTC)_2$ from the coordination interactions between triangular BTC^{3-} bridging ligands and Zn^{2+} ions is investigated using FTIR spectroscopy. As shown in Figure 1a, the H_3BTC linkers exhibit a strong, broad OH stretching band corresponding to the carboxylic groups at 3364 cm^{-1} .²² The broad absorption features between 3000 and 2600 cm^{-1} can be assigned to the C–H stretching vibrations. The

C=O and C–O vibrational modes of the carboxylic groups are observed at 1735 and 1390 cm^{-1} , respectively. After the coordination reaction with Zn^{2+} ions, the broad absorption bands of H_3BTC at 3000 – 2500 cm^{-1} vanish, while the OH band blueshifts and becomes more intense and broader. This OH band can be assigned to the asymmetric and symmetric vibrations of the coordinated water molecules in the $Zn_3(BTC)_2$ structure.²³ The absorption bands associated with the carbonyl groups also appear at lower and higher wavenumbers of 1665 and 1414 cm^{-1} , respectively, than those observed for the H_3BTC linker. These shifts suggest the complex formation of $Zn_3(BTC)_2$ through the deprotonation and coordination of the carboxylic groups with Zn^{2+} ions.²⁴ The absence of the absorption band corresponding to the –COOH groups around 1700 cm^{-1} also implies the complete deprotonation of the H_3BTC linkers after metal binding upon the binding of Zn^{2+} ions.²⁰ Moreover, the presence of the Zn–O stretching vibrations corresponding to the octahedral coordinated zinc center is confirmed by the absorption band at 756 cm^{-1} .²³

The powder XRD pattern of the as-synthesized $Zn_3(BTC)_2$ is presented in Figure 1b, while the details of the Bravais lattice parameter are given in Table S1. Compared with the simulated XRD pattern of $Zn_3(BTC)_2$ obtained from the Cambridge Crystallographic Data Centre (CCDC no. 664416), the as-synthesized sample exhibits quite distinctly different crystalline features, particularly for the Bragg reflections observed at higher 2θ angles of 15 – 40° . The relatively weak yet well-resolved reflections at higher Bragg angles may represent the impurity phases with smaller crystallite domains. The most intense (102) reflection located at $2\theta = 10.44^\circ$ in the experimental XRD pattern, however, well matches the simulated one ($2\theta = 10.37^\circ$). In addition, the two reflections that appear at $2\theta = 9.33$ and 12.71° are also the typical crystal features of $Zn_3(BTC)_2$.²³ This result thus suggests that the resultant product may contain multiphases, especially for the peaks at low Bragg angles of 9.39 , 10.44 , and 10.78° . The unit cell dimensions (Table S2) from the obtained XRD pattern show the triclinic crystal geometry of $Zn_3(BTC)_2$. The average crystallite size (D) obtained from the Scherer equation for the strongest (102) reflection was 8.5 nm .

The N_2 adsorption–desorption isotherms of $Zn_3(BTC)_2$ at 77 K show a typical IUPAC Type I(a)/II hybrid characteristic with well-defined steps at low and high relative pressures (Figure 1c). The significant uptake of N_2 in the low relative pressure region ($P/P_0 < 0.05$) can be attributed to the volume filling of narrow micropores in the MOF structure. The second steep uptake observed at high relative pressures ($P/P_0 > 0.95$) of the isotherms may reflect the multilayer adsorption of N_2 on the large mesopores and the external surface (i.e., macropores) of the samples,²⁵ thus characterizing the hierarchical architecture of porosity of $Zn_3(BTC)_2$. The presence of large mesopores and macropores inside the MOF material can facilitate the mass transport of large-sized reactant molecules into the catalytically active Lewis acid Zn^{2+} sites and desorption of products from the porous framework. The BET surface area (S_{BET}) and total pore volume (V_T) of $Zn_3(BTC)_2$ were found to be $1175.81\text{ m}^2\text{ g}^{-1}$ and $0.81\text{ cm}^3\text{ g}^{-1}$, respectively. Compared to the mesoporous Zn-BTC MOF ($S_{BET} = 12$ – $50\text{ m}^2\text{ g}^{-1}$) reported in the Wang et al. work,²³ the much higher S_{BET} of the $Zn_3(BTC)_2$ particles synthesized in this work can be ascribed to the existence of a micro/macroporous structure. In this regard, the high surface area of

Table 1. ANOVA Results for the FAME Yield Response at an Optimal Zn₃(BTC)₂ Loading of 1 Wt %

factor ^a	SS ^b	coef. estimated (α)	DF ^c	MS ^d	F value	P value ^e
model	1036.73	79.80	9	115.19	68.79	<0.0001*
<i>Linear effect</i>						
X ₁	156.65	4.42	1	156.65	93.54	<0.0001*
X ₂	559.49	9.15	1	559.49	334.10	<0.0001*
X ₃	162.73	4.22	1	162.73	97.17	<0.0001*
<i>Interaction effect</i>						
X ₁ X ₂	11.87	-1.86	1	11.87	7.09	0.0374*
X ₁ X ₃	23.14	2.24	1	23.14	13.82	0.0099*
X ₂ X ₃	4.49	-1.14	1	4.49	2.68	0.1525 ^{NS}
<i>Quadratic effect</i>						
X ₁ ²	0.7665	0.4642	1	0.7665	0.4577	0.5239 ^{NS}
X ₂ ²	236.24	-9.11	1	236.24	141.07	<0.0001*
X ₃ ²	16.26	-2.26	1	16.26	9.71	0.0207*
residual	10.05		6	1.67		
lack of fit	10.05		5	2.01		0.7218 ^{NS}
pure error	0.0000		1	0.0000		
corrected total	1046.78		15			
std. dev.	mean		R ²	adj. R ²	pred. R ²	precision
1.29	75.05		0.9904	0.9760	0.9113	29.6294

^aX₁ = reaction time (h); X₂ = methanol/oil molar ratio; X₃ = reaction temperature (°C). ^bSS = sum of squares. ^cDF = degree of freedom. ^dMS = mean squares. ^e* = statistically significant; NS = not significant.

the Zn₃(BTC)₂ particles with a significant micropore contribution (~60% of the S_{BET}, Table S3) would benefit the catalytic reaction by affording abundant OMSs, which allow the reactant molecules (i.e., triglycerides/free fatty acids and methanol) to interact more frequently with these active sites and promote the conversion efficiency toward the reaction product.

The TGA curve of Zn₃(BTC)₂ reveals a two-step thermal degradation process, as shown in Figure 1d. A mass loss (8.7%) observed below 100 °C could be attributed to the evaporation of the adsorbed moisture and the elimination of the lattice water molecules in the framework structure. The TGA curve shows a negligible weight loss between 100 and 270 °C, which denotes the absence of any coordinated DMF molecules after the activation process; the elimination of the DMF molecules occurs in the temperature range of 100–170 °C under a N₂ atmosphere.²⁶ The as-synthesized MOF possesses good thermal stability with no appreciable weight loss (<2 wt %) up to 300 °C. This result unambiguously confirms that the Zn₃(BTC)₂ MOF is thermally stable and does not lose its crystalline order or undergo structural collapse during the transesterification reaction at low temperatures (45–65 °C). The representative examples of MOF materials possessing good thermal stability and applied to the transesterification and esterification reactions can be found in Table S4. Upon increasing the temperature above 300 °C, a rapid weight loss (~40%) was observed, which reflects the collapse of the framework structure of Zn₃(BTC)₂ due to the decomposition of organic linkers. The weight loss profile reaches a plateau at temperatures between 400 and 600 °C, yielding a residual crystalline ZnO around 40 wt %. Beyond 600 °C, neither weight loss nor phase transition of the ZnO particles was observed, which is in good agreement with previous reports.^{20,27}

The SEM image of the Zn₃(BTC)₂ particles shows a nonisometric and triclinic morphology with relatively broad size distributions from 0.3 to 3.5 μm (Figure 1e,f). The observed discrepancy between the crystallite and particle sizes

measured from the XRD and SEM image may suggest that the resultant products are polycrystalline. The morphology of the Zn₃(BTC)₂ particles is also somewhat different from that reported earlier for a similar method.²⁸ A possible explanation for this morphological difference is due to the variation of the solvothermal synthetic conditions in the Zn₃(BTC)₂ system, such as the solvent type, metal salt, precursor molar ratio, temperature, reaction time, and others. Compared to the rod morphology reported by Wang et al.,²³ the addition of triethylamine as a co-solvent was not included in the present approach. Feng et al. also reported the rod-shaped Zn₃(BTC)₂ particles through a solvothermal method using ethanol-water.²⁸ Hao et al. demonstrated that the pore size and framework topology of Zn₃(BTC)₂ can be modulated by the solvent molecular size.²⁹ The results of the SEM observation are in agreement with the powder XRD pattern.

2.2. Effect of the Catalyst Loading on the FAME Yield.

The optimization of the catalyst loading is pivotal not only to maximize the reaction yield but also to minimize the production cost. Thus, the dependence of the catalyst loading on the yield of FAMEs was examined through a one-factor-at-a-time (OFAT) optimization method. The OFAT approach was selected due to its simplicity and with the consideration of excluding the catalyst loading factor from the intrinsic reaction parameters. As shown in Figure S1, a volcano-like relationship between the catalyst loading and FAME yield was observed, where the maximum conversion of 84.4% was accomplished at a catalyst load of 1 wt %. At a 0.5 wt % Zn₃(BTC)₂ catalyst loading, the simultaneous conversion of triglycerides and free fatty acids into FAMEs reaches about 80%. As the catalyst loading increased to the optimal value, the FAME yield slightly rose from 80 to 84.4%, which can be explained by the increased availability of the Lewis acid sites of Zn₃(BTC)₂, thus favoring the conversion of the reactant. The FAME conversion gradually declined upon increasing the catalyst concentration beyond 1 wt %. This phenomenon may be attributed to the decrease of the dispersion of active centers that hinder the molecular interactions between the reactants

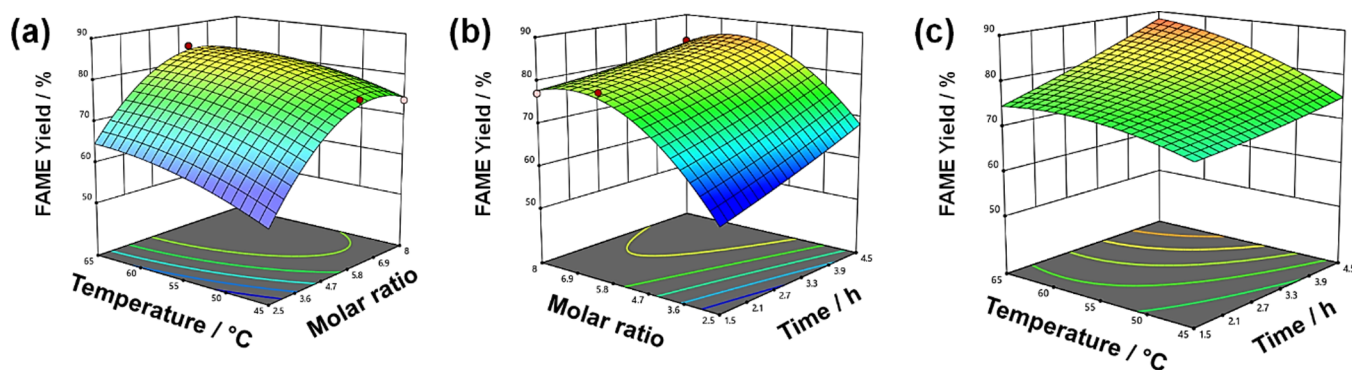


Figure 2. The 3D surface mesh plots with contour lines underneath illustrating the binary interaction effects of the independent reaction parameters on the ester yield: (a) temperature (X_3) and methanol/oil molar ratio (X_2), (b) methanol/oil molar ratio (X_2) and time (X_1), and (c) time (X_1) and temperature (X_3).

and active sites.³⁰ The blank reaction test without a catalyst under the same conditions shows no appreciable formation of FAMEs, affording only $\sim 3\%$ yield. This result confirms the indispensable role of catalysts in accelerating the transesterification reaction rate by decreasing the free energy barrier (ΔG^\ddagger).

2.3. Optimization and Modeling Studies of Biodiesel Production. The analysis of variance (ANOVA) results showing the effects of linear, quadratic, and interaction terms of the three investigated reaction parameters (i.e., reaction time (X_1), methanol/oil molar ratio (X_2), and reaction temperature (X_3)) on the FAME yield are summarized in Table 1. The statistical significance of the coefficient of each model term was examined through the Fisher's exact (F value) and probability (P value) tests, where P values less than 0.05 are considered statistically significant. Our preliminary analysis based on the P value, goodness of fit (R^2), and lack of fit suggested that the quadratic polynomial model is the most suitable for describing the response values compared to the linear and cubic functions. Based on this significance testing, the quadratic polynomial model (eq 1) was found to be appropriate and statistically acceptable at the 95% confidence level (P value < 0.0001) with an insignificant lack of fit (P value > 0.05) for predicting FAME yields. Moreover, the predicted results agree well with those obtained from the experiments (see Table 1), with the satisfactorily adjusted coefficient of determination (adj. R^2) of 0.976. This value implies that 97.6% of the FAME yield response variability could be described well by the model. Figure S2 also shows that all the data points lie close to the 45° reference line. The predicted R^2 value of 0.91 may reflect that the obtained model adequately approximates the response values under the experimental range studied without overfitting. Furthermore, the very low value of the coefficient of variation ($CV = 1.72\%$) and the considerably high adequate precision (i.e., signal-to-noise ratio > 4) point out that the model provides an accurate fit of the observed response and can navigate the design space.^{31,32}

The ANOVA test results reveal that all the linear, quadratic, and interaction parameters are statistically significant in the implemented model with P values lower than 0.05 (highlighted with an asterisk (*) in Table 1), except for the quadratic X_1^2 ($P = 0.5239$) and interactive X_2X_3 effects ($P = 0.1525$). The linear effect of the methanol/oil molar ratio (X_2) emerges as the most important contributor to increasing FAME yields ($P < 0.0001$ and F value = 334.1) among the other linear effects,

namely, reaction temperature (F value = 97.17) and time (F value = 93.54). The same trend was also observed for the square terms of reaction parameters, where X_2^2 (F value = 141.07) $> X_3^2$ (F value = 9.71) $> X_1^2$ (F value = 0.46). The optimal polynomial regression model after discarding the insignificant model terms (i.e., X_1^2 and X_2X_3) are expressed in eq 1 with respect to the coded variables.

$$\begin{aligned} \text{FAME yield (\%)} = & 79.80 + 4.42X_1 + 9.15X_2 + 4.22X_3 \\ & - 1.86X_1X_2 + 2.24X_1X_3 - 9.11X_2^2 \\ & - 2.26X_3^2 \end{aligned} \quad (1)$$

In eq 1, the positive and negative signs of the model terms represent the synergistic and antagonistic behavior, respectively. It can be seen that all the main effects (i.e., X_1 , X_2 , and X_3) have positive coefficients, suggesting that an increase of the reaction time, methanol/oil molar ratio, and temperature leads to higher reaction yields in the biodiesel production catalyzed by $\text{Zn}_3(\text{BTC})_2$. A more positive value of X_2 factor ($\alpha_2 = 9.15$) confirms the more significant role of the methanol/oil molar ratio in maximizing the FAME conversion rather than the reaction time ($\alpha_1 = 4.42$) and temperature ($\alpha_3 = 4.22$), which will be discussed in more detail in the next section. The positive coefficient of X_1X_3 ($\alpha_{13} = 2.24$) suggests the mutualistic effects between the reaction time and temperature in facilitating the conversion rate and yield of FAMEs. On the contrary, the negative signs for the X_1X_2 , X_2^2 , and X_3^2 significant model terms demonstrate the antagonistic effect of the square terms of the methanol/oil molar ratio and reaction temperature on the DPO conversion to biodiesel.

2.4. Parametric Study of the Biodiesel Production.

2.4.1. Effect of the Methanol/Oil Molar Ratio. Based on the ANOVA results, the methanol/oil molar ratio has the strongest influence on the FAME production in the presence of $\text{Zn}_3(\text{BTC})_2$. To further verify the significant influence of this factor, the interactions between the methanol/oil molar ratio and temperature (X_2X_3) or time (X_2X_1) in promoting FAME conversion are investigated, as portrayed in Figure 2a,b. As can be seen from the response surface plots, the curvature tends to be elliptical in shape, which indicates a significant interaction between each axis variable to the FAME response yield.³³ The increase in the molar ratio of methanol to DPO from 4:1 to 6:1 positively affects the FAME production. This can be simply explained by the fact (and in accord with Le Chatelier's principle) that an excess amount of alcohol is required to drive

the chemical equilibrium toward the product side. However, further increasing the methanol/oil molar ratio from 6:1 to 8:1 results in lower FAME yields. In this regard, the presence of excess methanol may encapsulate some active sites of the catalyst, leading to the hindered dipole interactions between the catalytically active sites with TG and FFA.³⁴ Moreover, the excessive methanol loading can promote the emulsification of the reaction mixture due to a recombination of FAMES and glycerol to produce monoglycerides,^{35,36} thus hindering the separation process of the product. Also, a large excess of methanol can improve the solubility of glycerol in the FAME-rich phase, which could adversely affect the purity and yield of the final biodiesel product. Thus, optimizing the methanol/oil molar ratio in the transesterification process is crucial not only for maintaining the high conversion efficiency of FAMES and product quality but also for minimizing the operating cost for unreacted methanol recovery.

2.4.2. Effects of the Reaction Temperature and Time. The interaction effect between the reaction temperature and time (X_3X_1) on FAME productivity is presented in Figure 2c. From the 3D response surface plot, it can be observed that the reaction temperature and time play a less significant role in modulating the FAME conversion efficiency compared to the methanol/oil molar ratio. The transesterification and esterification reactions are both endothermic and reversible, and thus, an increase in temperature provides more energy to the reaction mixture that shifts the chemical equilibrium in favor of the FAME formation. The elevated reaction temperatures also help to decrease the mass-transfer limitation between the methanol and oil phases, leading to the enhanced adsorption and diffusion of reactant molecules toward the catalytically active sites.³⁷ Meanwhile, a prolonged reaction time improves the FAME production, allowing a greater number of reactant molecules to be consumed and converted to FAMES over the catalyst surface. However, a further increase in the reaction temperature and time beyond their optimum conditions has negligible effects on the ester yield and may incur additional cost and energy requirements of the process.⁸

2.5. FAME Compositions and Fuel Properties of the DPO-Derived Biodiesel. Based on the above statistical optimization study, the maximum yield of biodiesel obtained from the one-step transesterification and esterification reactions of DPO over $Zn_3(BTC)_2$ was achieved at a methanol/oil molar ratio of 6:1, temperature of 65 °C, and reaction time of 4.5 h. The percent yield of biodiesel obtained from the second-order polynomial model prediction (eq 1) under these optimized reaction conditions was found to be 89.96%, which agrees remarkably well with the experimental value of 89.89% (see Table 4, entry 12). The total mass fractions of the FAME species in the product were 95 wt %, with predominantly palmitic and oleic acid methyl esters present (see Figure S3 for details on the FAME concentration profiles and the corresponding GC–FID chromatogram). The fuel properties of the DPO-derived biodiesel are presented in Table 2, which conform to the quality standard requirements specified in ASTM D6751 and the Indonesian National Standard (SNI 7182-2015), thereby suggesting the potential use of the as-produced biodiesel as either a neat fuel or petroleum diesel blends.

2.6. Catalyst Reusability and Catalytic Performance Comparison of $Zn_3(BTC)_2$. Reusability is an important aspect to consider when evaluating the robustness of a heterogeneous solid catalyst and its commercial potential, particularly from

Table 2. Fuel Properties of the Biodiesel Obtained from DPO along with a Comparison to the ASTM D6751 and SNI 7182-2015 Standard Specifications

fuel specifications	unit	ASTM D6751 ^a	SNI ^b	DPO biodiesel
acid value	mg KOH/g	0.50 max	0.50 max	0.36
cetane number		47 min	51 min	58.7 min
cloud point	°C	report	18 max	−11
density at 40 °C	kg/m ³	NS	850–890	885
flashpoint	°C	100–170	100 min	148
kinematic viscosity at 40 °C	mm ² /s	1.9–6.0	2.3–6.0	5.44
moisture content	ppm	NS	500 max	291

^aASTM: American Society for Testing and Materials; NS = not specified. ^bSNI: Indonesian National Standard.

economic and practical viewpoints. In this regard, the catalytic stability of $Zn_3(BTC)_2$ was assessed for up to five reaction cycles under optimal reaction conditions. As depicted in Figure 3a, the FAME yields were maintained at 85–90% over three consecutive runs but then gradually decreased to ~80 and ~75% at the fourth and fifth cycles, respectively. Such a decline in the catalytic activity could be attributed to the partial blocking of active catalytic sites by the surface adsorbed oil residue and byproduct (glycerol) molecules or the decreased Lewis acidic OMSs present in the MOF from the leaching event. To confirm the correlation between the activity decrease and metal leaching, we carried out flame atomic absorption spectroscopic (FAAS) measurements of FAME- and glycerol-rich layers at the end of each catalytic cycle. The results indicate that no appreciable leaching of the Zn metal (<5% with respect to the initial content in the catalyst) into the reaction mixture occurred during the first three reuse experiments. In comparison, a more pronounced Zn leaching takes place in the fourth (8.7%) and fifth (12.1%) catalytic cycles (see Figure S4).

We also compare the catalytic performance of $Zn_3(BTC)_2$ in the conversion of triglycerides and fatty acids to alkyl esters through the trans/esterification routes with other MOF materials reported in the literature.^{8,38–40} To provide a valid comparison and to better reflect the intrinsic activity of the as-prepared MOF catalyst, the turnover frequency (TOF), herein defined as the moles of the reactant converted per mole of the catalyst per hour,⁴¹ was employed in the comparative performance evaluation. Determining the identity and number of active sites can be difficult in the MOF composite catalysts; thus, the moles of the catalyst were used instead of the number of active catalytic sites for the calculation of TOF values.⁴² As shown in Figure 3b, the $Zn_3(BTC)_2$ exhibits a high intrinsic catalytic activity with a TOF value of 18.2 h^{−1}, which is comparable and/or exceeds that of the MOF materials reported by others.^{38–40} For example, the intrinsic catalytic activity and stability of $Zn_3(BTC)_2$ are superior to those of Co(II) MOF(1) (TOF = 2.0 h^{−1}) and NH₂-MIL-101(Cr)-Sal-Zr (TOF = 13.5 h^{−1}) in the transesterification of plant oil and esterification of oleic acid, respectively, albeit with the use of lower catalyst loading and methanol/oil molar ratio. The as-prepared catalyst also exhibits an intrinsic activity comparable to that of Fe₃O₄@NH₂-MIL-88B(Fe) MOF functionalized by the Brønsted ionic liquid DAIL (TOF = 17.5 h^{−1}) for the

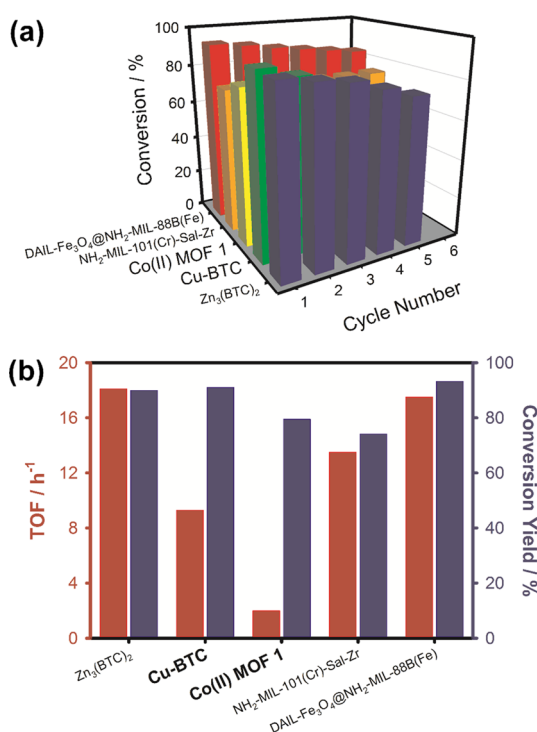


Figure 3. (a) Recyclability of the $Zn_3(BTC)_2$ catalyst for the simultaneous transesterification–esterification of DPO under optimized reaction conditions (i.e., methanol/oil molar ratio = 6:1; temperature = 65 °C; time = 4.5 h) along with its catalytic performance compared to the other MOF materials previously reported for FAME production, such as DAIL-Fe₃O₄@NH₂-MIL-88B(Fe), NH₂-MIL-101(Cr)-Sal-Zr, Co(II) MOF 1, and Cu-BTC. The recovery and reuse experiments of the MOF catalysts in the present work and cited studies were performed according to the procedure described in Section 4.4, with slight variations in the separation process and drying conditions. Note that the catalytic activity of the representative MOF materials over several cycles in the 3D bar chart was redrawn and presented based on the corresponding literature data. (b) Comparison of the intrinsic activity (TOF) of the as-synthesized $Zn_3(BTC)_2$ and other MOF catalysts in the transesterification and esterification reactions, along with the achieved conversion yield.

esterification of oleic acid with methanol, while also affording milder and more economical reaction conditions, such as lower methanol/oil molar ratio, temperature, and catalyst loading. Moreover, it is important to remark that the solvothermal preparation of $Zn_3(BTC)_2$ MOF is quite simple and involves less expensive precursor chemicals (including an organic linker) than the abovementioned MOF materials, thus presenting an economic benefit. Taken together, these results suggest the great potential of the $Zn_3(BTC)_2$ MOF with abundant active sites as an efficient, high-activity, and robust catalyst for the one-step transesterification and esterification reactions.

2.7. Proposed Mechanism for the One-Step Transesterification–Esterification Reaction of DPO. The proposed mechanism for the one-step transesterification–esterification reaction of DPO to FAMEs is illustrated in Figure 4. In this kind of reaction, the preactivated $Zn_3(BTC)_2$ with open and unsaturated metal centers acts as a mediator that facilitates the convergence of methanol and DPO, resulting in biodiesel conversion.^{43,44} These active sites can facilitate the adsorption of reactant species (i.e., triglycerides

and methanol) by forming coordination reactions via the interface dipole,^{45,46} electron delocalization,⁴⁷ or nucleophilic attack.⁴⁸

The reaction mechanism steps are explained in details as follows:

Step 1: The TG (RCOOR' as monoglycerides) and FFA (RCOOH) species present in the DPO bind to the central hexa-coordinated zinc atom via their carbonyl oxygen atom, resulting in the formation of carbocation intermediates. The formation of Zn–O bonding could be ascribed to the presence of the dipole on the metal surfaces and the protonation of oleic acid (taken as representative of FFA). At the same time, methanol molecules may also bind to the unsaturated metal sites. Then, a nucleophilic attack occurs between the two neighboring molecules.

Steps 2: In the esterification reaction pathway, FAME (RCOOCH₃) conversion occurs along with water molecules. Meanwhile, the transesterification of monoglycerides involves a proton (H⁺) transfer to the ester group (R'O) to produce glycerol (R'OH) through the delocalization of the oxygen atom.

Step 3: The resulting FAME molecules are desorbed from the catalyst through the electron delocalization at the oxygen atom, where FAMEs as the main product are collected, and the catalyst can be reused for the next catalytic run after regeneration treatment.

2.8. Cost Analysis of the $Zn_3(BTC)_2$ Synthesis. The biodiesel production economics depend predominantly on the direct operating cost (DOC), which reflects the costs of raw materials (i.e., feedstock oil, alcoholic reaction solvent, and catalyst) and the operating labors. According to the previous cost analysis study by You et al.,⁴⁹ the catalyst cost represents the second most significant proportion of the DOC after the cost of the feedstock oil. Accordingly, a great economic advantage in the commercial-scale biodiesel production, aside from utilizing low-grade fatty feedstocks, can also be realized using efficient, low-cost, and reusable solid catalysts. In this section, we examined the economics and energy cost of the kilogram-scale solvothermal synthesis of the $Zn_3(BTC)_2$ catalyst based on the reaction conditions and process steps demonstrated at the laboratory scale (see Section 4.3). The metal salt and organic linker precursors, reaction solvent, and necessary capital equipment in each process step (i.e., synthesis, filtration, activation, and drying) are presented in Table 3 along with their price quotes in US dollars, unless otherwise noted.

The cost evaluation results demonstrate that the production cost of the $Zn_3(BTC)_2$ catalyst is about US\$51 per kg, which is found to be considerably cheaper than those of commercial acidic ion-exchange resin catalysts, such as Amberlyst 15 (~US\$100 per kg), Amberlyst 36 (~US\$120 per kg), and Purolite D5081/CT175 (~US\$120 per kg). Moreover, compared with the production costs of representative MOFs reported in Figure 3a, the synthesis of $Zn_3(BTC)_2$ is intrinsically more affordable by considering (i) the less expensive bridging organic ligands (the linker price can be found in Table S5), (ii) milder solvothermal reaction conditions, and (iii) fewer synthesis steps. A technoeconomic analysis of the solvothermal MOF synthesis reported by DeSantis and coworkers has identified that the linker costs are the second largest contributor to the MOF production costs after the organic solvents.⁵⁰ Although the production cost of $Zn_3(BTC)_2$ is expected to be higher than those of heterogeneous solid base

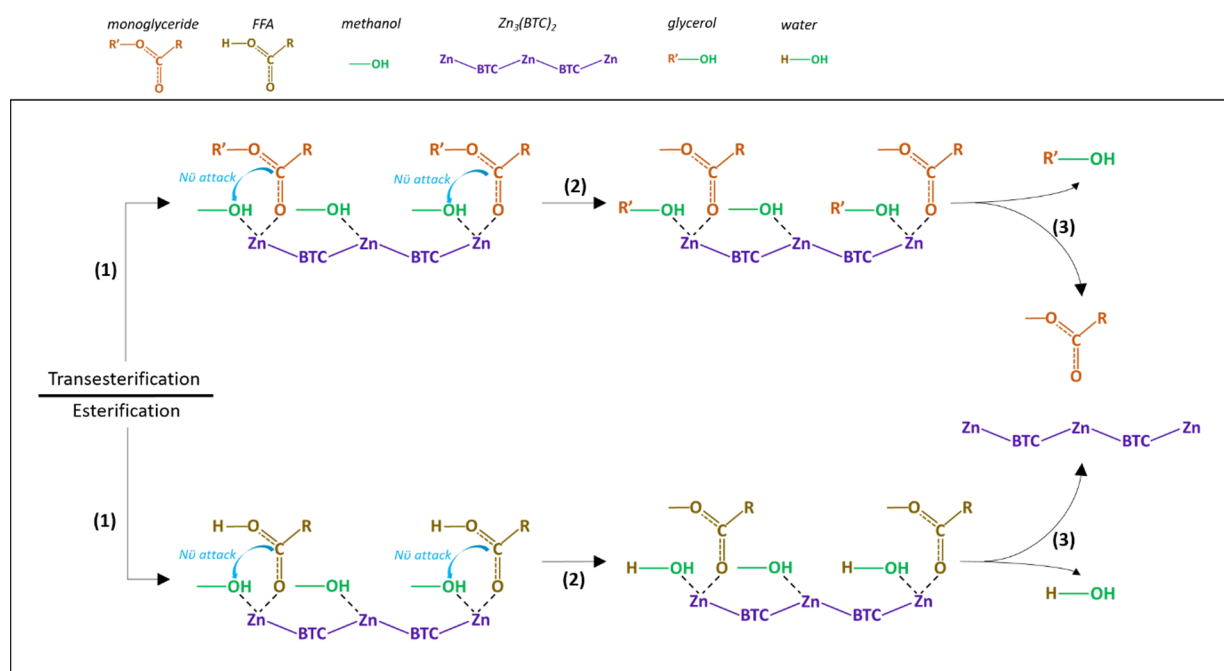


Figure 4. Proposed mechanism for the one-step transesterification and esterification reactions of DPO over the $\text{Zn}_3(\text{BTC})_2$ MOF catalyst.

Table 3. Detailed DOC for the Solvothermal Synthesis of $\text{Zn}_3(\text{BTC})_2$ on the Kilogram Scale

DOC	specification	price (US\$ kg^{-1})	amount (kg) ^b	total (US\$)
chemicals^a				
1. $\text{ZnSO}_4 \cdot 7\text{H}_2\text{O}$	99.9%	5.6	2.0	11.2
2. H_3BTC	min 99%	20.0	0.9	18.0
3. DMF	min 99.9%	0.9	18	16.2
4. methanol	min 99.9%	0.35	4.0	1.4
5. H_2O	18.2 M Ω	0.1	14.0	1.4
Utility				
electricity		0.1 US\$ per kWh	20.0 kWh	2.0
Total DOC				50.2

^a H_3BTC = 1,3,5-benzenetricarboxylate; DMF = *N,N*-dimethylformamide. ^bThe estimated total amount of DMF solvent for the synthesis and washing steps. Methanol was used for the washing and activation steps.

catalysts, such as the alkaline earth metal oxides (CaO and MgO), the feasibility of using substantially cheaper low-quality or waste feedstock oils can lead to the lower overall cost of biodiesel production. A detailed economic cost analysis of the large-capacity biodiesel production is beyond the scope of this study, and the interested readers can refer to a comprehensive study by You et al.⁴⁹

3. CONCLUSIONS

In summary, we have demonstrated the catalytic utility of a Zn(II)-based carboxylate MOF ($\text{Zn}_3(\text{BTC})_2$) for the simultaneous transesterification and esterification of a low-grade vegetable oil (DPO) to biodiesel. The influential reaction parameters, including the methanol/oil molar ratio, temperature, and time, are optimized through the RSM–BBD method. A one-way ANOVA test points out a more significant role of the methanol/oil molar ratio over both temperature and time to achieve the maximum FAME conversion. Moreover, the reusability of the $\text{Zn}_3(\text{BTC})_2$ catalyst is also successfully demonstrated across five consecutive runs with only a marginal decrease in the FAME conversion. In addition, the following points represent the important results of this study:

- The solvothermally synthesized $\text{Zn}_3(\text{BTC})_2$ MOF exhibits a triclinic crystal structure with a hierarchical macro/microporous structure and Lewis acidic OMSs.
- The maximum biodiesel yield (89.9%) with a 95% DPO-to-FAME conversion was achieved under the optimum reaction conditions of a methanol/oil molar ratio = 6:1, temperature = 65 °C, and time = 4.5 h with the presence of a 1 wt % catalyst.
- The DPO-derived biodiesel properties satisfy the standard fuel specification requirements of ASTM6751 and SNI 7182-2015.
- The total DOC of the $\text{Zn}_3(\text{BTC})_2$ catalyst is estimated to be US\$50 per kg, which is less expensive than those of previously reported MOF materials and the benchmark acid resin catalysts.

4. EXPERIMENTS

4.1. Materials. Zinc sulfate heptahydrate ($\text{ZnSO}_4 \cdot 7\text{H}_2\text{O}$, $\geq 99.95\%$ trace metal basis), H_3BTC ($\text{C}_6\text{H}_3(\text{CO}_2\text{H})_3$, 98% purity), methanol (CH_3OH , anhydrous, $\geq 99.8\%$ purity), *n*-hexane (HPLC grade, $\geq 95\%$ purity), *N,N*-dimethylformamide (DMF, ACS reagent, $\geq 99.8\%$ purity), and the FAME reference

Table 4. RSM–BBD Experimental Design Showing the Coded and Actual Values of the Reaction Parameters in the Transesterification of DPO Using the Zn₃(BTC)₂ Catalyst

run	coded parameters ^a			response % FAME yield (Y)	
	time, h (X ₁)	methanol/oil molar ratio (X ₂)	temperature, °C (X ₃)	experimental	predicted
1	0 (3)	0 (6)	1 (65)	60.20	59.58
2	1 (4.5)	0 (6)	0 (55)	64.02	63.34
3	−1 (1.5)	−1 (4)	−1 (45)	63.98	64.21
4	−1 (1.5)	−1 (4)	1 (65)	68.60	69.20
5	0 (3)	0 (6)	0 (55)	72.80	73.76
6	0 (3)	0 (6)	0 (55)	73.93	74.12
7	1 (4.5)	−1 (4)	−1 (45)	69.89	70.24
8	1 (4.5)	−1 (4)	1 (65)	83.41	84.21
9	−1 (1.5)	0 (6)	0 (55)	79.62	78.17
10	0 (3)	0 (6)	−1 (45)	76.77	75.45
11	0 (3)	0 (6)	1 (65)	84.33	83.27
12	1 (4.5)	0 (6)	1 (65)	89.96	89.89
13	−1 (1.5)	1 (8)	0 (55)	77.12	77.75
14	0 (3)	1 (8)	−1 (45)	73.77	74.51
15	0 (3)	1 (8)	1 (65)	80.33	80.67
16	1 (4.5)	1 (8)	0 (55)	83.28	82.87
17	0 (3)	0 (6)	0 (55)	73.24	73.11

^aThe actual values of the coded parameters are given in parentheses.

standard mixture (Supelco 37-component FAME mix, 47885-U) were purchased from Sigma-Aldrich, Singapore, and used as received without further purification. Crude palm oil (CPO) was supplied by a local company in Surabaya, East Java (Bintang Era Sinar Tama, PT).

4.2. Degumming Pretreatment of CPO. CPO was degummed using a conventional dry method with phosphoric acid according to the procedure described elsewhere.⁵¹ The acid value (AV) and saponification value (SV) of DPO were determined to be 12.1 and 227.5 mg KOH/g, respectively, according to the AOCS official methods Cd-3d-63 and Cd-3-25. The average molecular weight of DPO was determined from the AV and SV using the equation described by Akusu et al.⁵² and found to be 780.1 g mol^{−1}. The fatty acid composition of DPO (Table S6) was determined using gas chromatography–flame ionization detector (GC–FID) analysis (GC-2014, Shimadzu, Japan) as described by Ong et al.⁵³ The labeling of fatty acid peaks in the chromatogram was performed by comparing their retention times with those of authentic standards.

4.3. Solvothermal Synthesis of Zn₃(BTC)₂. The one-pot solvothermal synthesis of Zn₃(BTC)₂ was carried out following a previously reported procedure with minor modifications.²³ Briefly, ZnSO₄·7H₂O (2.16 g, 7.51 mmol) and H₃BTC (1.05 g, 5.0 mmol) were dissolved in 30 mL of the DMF/H₂O (1/1; v/v) mixture and then magnetically stirred at 200 rpm for an hour at room temperature. Subsequently, the mixture was transferred to a Teflon-lined stainless steel autoclave and heated isothermally at 85 °C for 24 h. Afterward, the autoclave was gradually cooled to room temperature. The resultant white powder (~1.2 g; 76% molar yield based on Zn) was collected by vacuum filtration followed by washing with fresh DMF and anhydrous methanol to remove the unreacted starting material. The obtained Zn₃(BTC)₂ was activated using methanol reflux for 4 h followed by drying in an oven at 150 °C for 12 h.

4.4. Biodiesel Production. The catalytic activity of Zn₃(BTC)₂ was assessed for the simultaneous transesterification and esterification reactions of DPO in a batch mode. The methanol/oil molar ratios were varied from 4:1 to 6:1 to 8:1,

while the catalyst loading was adjusted to 0.5, 1.0, 3.0, and 5.0 wt % relative to the DPO. The mixtures were then heated to the desired temperatures (i.e., 45, 55, and 65 °C) using an electric heating mantle and held isothermally for 1.5, 3, and 4.5 h with continuous magnetic stirring at 500 rpm. After the reaction, the flask was quenched in an ice-water bath. The resulting products composed of the upper fatty acid methyl esters (FAMEs)-rich and lower glycerol-rich phases were separated by centrifugation at 4900 rpm for 5 min. The FAME compositional analysis was carried out by the GC–FID method described in our previous study.⁵³ The yield of FAMEs was determined based on the following equation:

$$\text{FAME yield (\%)} = \frac{\text{weight of biodiesel (g)}}{\text{weight of DPO (g)}} \times \text{FAME content} \quad (2)$$

$$\text{FAME content} = 100 \times \left(\frac{\sum A - A_{\text{IS}}}{A_{\text{IS}}} \right) \times \left(\frac{C_{\text{IS}} \times V_{\text{IS}}}{m} \right) \quad (3)$$

The FAME content was calculated as the sum of the integrated peak areas of all individual FAMEs identified in the samples ($\sum A$) according to eq 3.⁵⁴ The notations A_{IS} , C_{IS} , and V_{IS} denote the peak area, concentration, and volume of the methyl heptadecanoate (C17:0) solution as the internal standard, respectively. The spent catalyst powder was further collected by centrifugation and purified by multiple washing with *n*-hexane to remove any residual oil left on the catalyst surface. The recovered catalyst was dried under vacuum at 60 °C for 12 h and then used in the subsequent reaction cycles for the reusability test.

4.5. Material Characterizations. Characterizations of the as-synthesized Zn₃(BTC)₂ were carried out using field-emission scanning electron microscopy (FESEM), X-ray diffraction (XRD), thermogravimetric analysis (TGA), nitrogen (N₂) adsorption–desorption isotherms, and Fourier transform infrared (FTIR) spectroscopy. SEM images were collected using an FEI Inspect F50 at an accelerating voltage of

10 kV. XRD patterns were acquired using a Bruker D2 Phaser X-ray diffractometer equipped with a Cu $K\alpha$ radiation source ($\lambda = 0.15406$ nm) in the 2θ range of $10\text{--}50^\circ$ at a scan speed of $0.1^\circ/\text{s}$. N_2 adsorption–desorption measurements were conducted at -196°C using a Micromeritics ASAP 2020 analyzer. Prior to the sorption measurements, the sample was degassed at 200°C under vacuum for 12 h. The thermal stability of the catalyst was examined using a Perkin-Elmer TGA 8000 analyzer from 30 to 600°C with a heating ramp of $10^\circ\text{C}/\text{min}$ under a N_2 flow at $20\text{ mL}/\text{min}$. FTIR spectra were collected in transmission mode using a Shimadzu 8400S spectrometer in the wavenumber range of $4000\text{--}500\text{ cm}^{-1}$ with a KBr pellet method.

4.6. Design of Experiments and Mathematical Modeling. RSM based on the Box–Behnken design (BBD) was adopted to investigate the effects of the reaction parameters and their interactions toward optimizing a particular response. The mathematical modeling and statistical analysis were performed using the Design-Expert version 12 software (Stat-Ease Inc., Minneapolis, MN, USA). Three reaction parameters affecting the production of FAMES were investigated, namely, time (coded as X_1), methanol/oil molar ratio (coded as X_2), and temperature (coded as X_3). The experimental design was constructed using 17 runs with three levels for each parameter, including three replications at the center point, as presented in Table 4. The experimental data were then analyzed using a second-order polynomial response surface model as follows:

$$Y = \alpha_0 + \sum_{i=1}^K \alpha_i X_i + \sum_{i=1}^K \alpha_{ii} X_i^2 + \sum_{i=1}^K \sum_{j=i+1}^K \alpha_{ij} X_i X_j + e \quad (4)$$

where Y is the target response (i.e., % FAME yield), X_i is the coded levels of independent variables, α_0 is the regression constant, α_i is the linear term corresponding to the input factor X_i , α_{ij} corresponds to the interaction term between the input factors X_i and X_j , α_{ii} is the quadratic term of input factor X_i , and e is the experimental error value of Y . The term K represents the total number of experimental variables involved in the optimization of the response.

■ ASSOCIATED CONTENT

SI Supporting Information

The Supporting Information is available free of charge at <https://pubs.acs.org/doi/10.1021/acsomega.0c03826>.

- Bravais lattice parameter of $\text{Zn}_3(\text{BTC})_2$ (Table S1), unit cell parameters of $\text{Zn}_3(\text{BTC})_2$ (Table S2), textural properties of the $\text{Zn}_3(\text{BTC})_2$ (Table S3), representative MOF catalysts applied in the transesterification and esterification reactions (Table S4), cost details of the organic linkers used in the synthesis of representative MOFs (Table S5), fatty acid composition of DPO obtained from GC–FID analysis (Table S6), OFAT analysis of the $\text{Zn}_3(\text{BTC})_2$ catalyst loading (Figure S1), plot of actual vs predicted FAME yield response (Figure S2), GC–FID chromatogram and mass fraction of FAME species in DPO-derived biodiesel (Figure S3), leaching profiles of zinc metal post-usage of $\text{Zn}_3(\text{BTC})_2$ (Figure S4) (PDF)

■ AUTHOR INFORMATION

Corresponding Authors

Shella Permatasari Santoso – Department of Chemical Engineering, Widya Mandala Surabaya Catholic University, Surabaya 60114, Indonesia; orcid.org/0000-0003-4698-583X; Phone: +62 31 3891264; Email: shella_p5@yahoo.com; Fax: +62 31 3891267

Suryadi Ismadji – Department of Chemical Engineering, Widya Mandala Surabaya Catholic University, Surabaya 60114, Indonesia; Department of Chemical Engineering, National Taiwan University of Science and Technology, Taipei 10607, Taiwan; orcid.org/0000-0002-5005-2824; Phone: +62 31 3891264; Email: suryadiismadji@yahoo.com; Fax: +62 31 3891267

Authors

Valentino Bervia Lunardi – Department of Chemical Engineering, Widya Mandala Surabaya Catholic University, Surabaya 60114, Indonesia

Fransiska Gunawan – Department of Chemical Engineering, Widya Mandala Surabaya Catholic University, Surabaya 60114, Indonesia

Felycia Edi Soetaredjo – Department of Chemical Engineering, Widya Mandala Surabaya Catholic University, Surabaya 60114, Indonesia; Department of Chemical Engineering, National Taiwan University of Science and Technology, Taipei 10607, Taiwan

Chun-Hu Chen – Department of Chemistry, National Sun Yat-Sen University, Kaohsiung 80424, Taiwan; orcid.org/0000-0002-3512-6880

Maria Yuliana – Department of Chemical Engineering, Widya Mandala Surabaya Catholic University, Surabaya 60114, Indonesia; orcid.org/0000-0002-3915-9401

Alfin Kurniawan – Department of Chemistry, National Sun Yat-Sen University, Kaohsiung 80424, Taiwan; orcid.org/0000-0003-2867-355X

Jenni Lie – Department of Chemical Engineering, National Taiwan University of Science and Technology, Taipei 10607, Taiwan

Artik Elisa Angkawijaya – Graduate Institute of Applied Science and Technology, National Taiwan University of Science and Technology, Taipei 10607, Taiwan; orcid.org/0000-0002-4405-5068

Complete contact information is available at:

<https://pubs.acs.org/10.1021/acsomega.0c03826>

Author Contributions

[†]V.B. and F.G. have contributed equally to this work.

Notes

The authors declare no competing financial interest.

■ ACKNOWLEDGMENTS

This study was financially supported by the Ministry of Research and Technology/National Agency for Research and Innovation, the Republic of Indonesia, through a project with contract number 130C/WM01.5/N/2020. We also greatly appreciate the Department of Chemistry, National Sun Yat-Sen University (NSYSU), Taiwan, for the assistance in material characterization.

REFERENCES

- (1) Park, Y.-M.; Lee, D.-W.; Kim, D.-K.; Lee, J.-S.; Lee, K.-Y. The heterogeneous catalyst system for the continuous conversion of free fatty acids in used vegetable oils for the production of biodiesel. *Catal. Today* **2008**, *131*, 238–243.
- (2) Puna, J. F.; Gomes, J. F.; Correia, M. J. N.; Dias, A. P. S.; Bordado, J. C. Advances on the development of novel heterogeneous catalysts for transesterification of triglycerides in biodiesel. *Fuel* **2010**, *89*, 3602–3606.
- (3) Hara, M. Environmentally Benign Production of Biodiesel Using Heterogeneous Catalysts. *Chem. Sus. Chem.* **2009**, *2*, 129–135.
- (4) de Lima, A. L.; Ronconi, C. M.; Mota, C. J. A. Heterogeneous basic catalysts for biodiesel production. *Catal. Sci. Technol.* **2016**, *6*, 2877–2891.
- (5) Islam, M. K.; Wang, H.; Rehman, S.; Dong, C.; Hsu, H.-Y.; Lin, C. S. K.; Leu, S.-Y. Sustainability metrics of pretreatment processes in a waste derived lignocellulosic biomass biorefinery. *Bioresour. Technol.* **2020**, *298*, 122558.
- (6) Dong, C.; Wang, Y.; Wang, H.; Lin, C. S. K.; Hsu, H.-Y.; Leu, S.-Y. New Generation Urban Biorefinery toward Complete Utilization of Waste Derived Lignocellulosic Biomass for Biofuels and Value-Added Products. *Energy Procedia* **2019**, *158*, 918–925.
- (7) Marso, T. M. M.; Kalpage, C. S.; Udugala-Ganehenege, M. Y. Application of Chromium and Cobalt Terephthalate Metal Organic Frameworks as Catalysts for the Production of Biodiesel from *Calophyllum inophyllum* Oil in High Yield Under Mild Conditions. *J. Inorg. Organomet. Polym.* **2020**, *30*, 1243–1265.
- (8) Pangestu, T.; Kurniawan, Y.; Soetaredjo, F. E.; Santoso, S. P.; Irawaty, W.; Yuliana, M.; Hartono, S. B.; Ismadji, S. The synthesis of biodiesel using copper based metal-organic framework as a catalyst. *J. Environ. Chem. Eng.* **2019**, *7*, 103277.
- (9) Ali, B.; Yusup, S.; Quitain, A. T.; Alnarabiji, M. S.; Kamil, R. N. M.; Kida, T. Synthesis of novel graphene oxide/bentonite bi-functional heterogeneous catalyst for one-pot esterification and transesterification reactions. *Energy Convers. Manage.* **2018**, *171*, 1801–1812.
- (10) Nakpong, P.; Wootthikanokkhan, S. High free fatty acid coconut oil as a potential feedstock for biodiesel production in Thailand. *Renewable Energy* **2010**, *35*, 1682–1687.
- (11) Ruzich, N. I.; Bassi, A. S. Investigation of lipase-catalyzed biodiesel production using ionic liquid [BMIM][PF₆] as a co-solvent in 500 mL jacketed conical and shake flask reactors using triolein or waste canola oil as substrates. *Energy Fuels* **2010**, *24*, 3214–3222.
- (12) Valvekens, P.; Vermoortele, F.; de Vos, D. Metal-organic frameworks as catalysts: the role of metal active sites. *Catal. Sci. Technol.* **2013**, *3*, 1435–1445.
- (13) Nikseresht, A.; Daniyali, A.; Ali-Mohammadi, M.; Afzalnia, A.; Mirzaie, A. Ultrasound-assisted biodiesel production by a novel composite of Fe(III)-based MOF and phosphotangestic acid as efficient and reusable catalyst. *Ultrason. Sonochem.* **2017**, *37*, 203–207.
- (14) Zhang, Q.; Lei, D.; Luo, Q.; Wang, J.; Deng, T.; Zhang, Y.; Ma, P. Efficient biodiesel production from oleic acid using metal-organic framework encapsulated Zr-doped polyoxometalate nano-hybrids. *RSC Adv.* **2020**, *10*, 8766–8772.
- (15) Lien, Y.-S.; Hsieh, L.-S.; Wu, J. C. S. Biodiesel synthesis by simultaneous esterification and transesterification using oleophilic acid catalyst. *Ind. Eng. Chem. Res.* **2010**, *49*, 2118–2121.
- (16) Farzaneh, F.; Mortazavi, S. S. Zn metal organic framework as a heterogeneous catalyst for the alkylation of toluene with benzyl bromide. *Reac. Kinet. Mech. Cat.* **2017**, *120*, 333–344.
- (17) Huang, X.; Chen, Y.; Lin, Z.; Ren, X.; Song, Y.; Xu, Z.; Dong, X.; Li, X.; Hu, C.; Wang, B. Zn-BTC MOFs with active metal sites synthesized via a structure-directing approach for highly efficient carbon conversion. *Chem. Commun.* **2014**, *50*, 2624–2627.
- (18) Madasamy, K.; Kumaraguru, S.; Sankar, V.; Mannathan, S.; Kathiresan, M. A Zn based metal organic framework as a heterogeneous catalyst for C–C bond formation reactions. *New J. Chem.* **2019**, *43*, 3793–3800.
- (19) Sajjadifar, S.; Arzehgar, Z.; Ghayuri, A. Zn₃(BTC)₂ as a Highly Efficient Reusable Catalyst for the Synthesis of 2-Aryl-1H-Benzimidazole. *J. Chin. Chem. Soc.* **2017**, *65*, 205–211.
- (20) Yaghi, O. M.; Davis, C. E.; Li, G.; Li, H. Selective guest binding by tailored channels in a 3-D porous zinc(II)-benzenetricarboxylate network. *J. Am. Chem. Soc.* **1997**, *119*, 2861–2868.
- (21) Pentyala, V.; Davydovskaya, P.; Ade, M.; Pohle, R.; Urban, G. Metal-organic frameworks for alcohol gas sensor. *Sensor. Actuat. B-Chem.* **2015**, *222*, 904–909.
- (22) Mahalakshmi, G.; Balachandran, V. FT-IR and FT-Raman spectra, normal coordinate analysis and ab initio computations of Trimesic acid. *Spectrochim. Acta A* **2014**, *124*, 535–547.
- (23) Wang, X.; Ma, X.; Wang, H.; Huang, P.; Du, X.; Lu, X. A zinc(II) benzenetricarboxylate metal organic framework with unusual adsorption properties, and its application to the preconcentration of pesticides. *Microchim. Acta* **2017**, *184*, 3681–3687.
- (24) da Silva, C. T. P.; Safadi, B. N.; Moisés, M. P.; Meneguim, J. G.; Arroyo, P. A.; Fávoro, S. L.; Giroto, E. M.; Radovanovic, E.; Rinaldi, A. W. Synthesis of Zn-BTC metal organic framework assisted by a home microwave oven and their unusual morphologies. *Mater. Lett.* **2016**, *182*, 231–234.
- (25) To, J. W. F.; Chen, Z.; Yao, H.; He, J.; Kim, K.; Chou, H.-H.; Pan, L.; Wilcox, J.; Cui, Y.; Bao, Z. Ultrahigh Surface Area Three-Dimensional Porous Graphitic Carbon from Conjugated Polymeric Molecular Framework. *ACS Cent. Sci.* **2015**, *1*, 68–76.
- (26) Chanthapally, A.; Oh, W. T.; Vittal, J. J. [2 + 2] Cycloaddition reaction as a tool to monitor the formation of thermodynamically stable ladder coordination polymers. *CrystEngComm* **2013**, *15*, 9324–9327.
- (27) Noack, V.; Eychmüller, A. Annealing of Nanometer-Sized Zinc Oxide Particles. *Chem. Mater.* **2002**, *14*, 1411–1417.
- (28) Feng, C.; Cao, X.; Zhang, L.; Guo, C.; Akram, N.; Wang, J. Zn 1,3,5-benzenetricarboxylate as an efficient catalyst for the synthesis of cyclic carbonates from CO₂. *RSC Adv.* **2018**, *8*, 9192–9201.
- (29) Hao, X.-R.; Wang, X.-L.; Shao, K.-Z.; Yang, G.-S.; Su, Z.-M.; Yuan, G. Remarkable solvent-size effects in constructing novel porous 1,3,5-benzenetricarboxylate metal-organic frameworks. *Cryst. Eng. Comm.* **2012**, *14*, 5596–5603.
- (30) Han, M.; Li, Y.; Gu, Z.; Shi, H.; Chen, C.; Wang, Q.; Wan, H.; Guan, G. Immobilization of thiol-functionalized ionic liquids onto the surface of MIL-101(Cr) frameworks by S-Cr coordination bond for biodiesel production. *Colloid Surf. A Physicochem. Eng. Asp.* **2018**, *553*, 593–600.
- (31) Temel, F.; Kutluay, S. Investigation of high-performance adsorption for benzene and toluene vapors by calix[4]arene based organosilica (CBOS). *New J. Chem.* **2020**, *44*, 12949–12961.
- (32) Sen, S.; Mondal, U.; Singh, G. Dual Optimization in Phase Transfer Catalyzed Synthesis of Dibenzyl Sulfide using Response Surface Methodology. *Org. Process Res. Dev.* **2016**, *20*, 1765–1773.
- (33) Singh, V.; Belova, L.; Singh, B.; Sharma, Y. C. Biodiesel production using a novel heterogeneous catalyst, magnesium zirconate (Mg₂Zr₃O₁₂): Process optimization through response surface methodology (RSM). *Energy Convers. Manage.* **2018**, *174*, 198–207.
- (34) Amouhadi, E.; Fazaeli, R.; Aliyan, H. Biodiesel production via esterification of oleic acid catalyzed by MnO₂@Mn(btc) as a novel and heterogeneous catalyst. *J. Chin. Chem. Soc.* **2019**, *66*, 608–613.
- (35) Encinar, J. M.; González, J. F.; Rodríguez-Reinares, A. Ethanolysis of used frying oil. Biodiesel preparation and characterization. *Fuel Process. Technol.* **2007**, *88*, 513–522.
- (36) Liu, Y.; Wang, L.; Yan, Y. Biodiesel synthesis combining pre-esterification with alkali catalyzed process from rapeseed oil deodorizer distillate. *Fuel Process. Technol.* **2009**, *90*, 857–862.
- (37) Sievers, C.; Noda, Y.; Qi, L.; Albuquerque, E. M.; Rioux, R. M.; Scott, S. L. Phenomena Affecting Catalytic Reactions at Solid-Liquid Interfaces. *ACS Catal.* **2016**, *6*, 8286–8307.
- (38) Wu, Z.; Chen, C.; Wan, H.; Wang, L.; Li, Z.; Li, B.; Guo, Q.; Guan, G. Fabrication of Magnetic NH₂-MIL-88B (Fe) Confined

Brønsted Ionic Liquid as an Efficient Catalyst in Biodiesel Synthesis. *Energ. Fuel.* **2016**, *30*, 10739–10746.

(39) Hassan, H. M. A.; Betiha, M. A.; Mohamed, S. K.; El-Sharkawy, E. A.; Ahmed, E. A. Salen-Zr(IV) complex grafted into amine-tagged MIL-101(Cr) as a robust multifunctional catalyst for biodiesel production and organic transformation reactions. *Appl. Surf. Sci.* **2017**, *412*, 394–404.

(40) Peña-Rodríguez, R.; Márquez-López, E.; Guerrero, A.; Chiñas, L. E.; Hernández-González, D. F.; Rivera, J. M. Hydrothermal synthesis of cobalt (II) 3D metal-organic framework acid catalyst applied in the transesterification process of vegetable oil. *Mater. Lett.* **2018**, *217*, 117–119.

(41) Kozuch, S.; Martin, J. M. L. “Turning Over” Definitions in Catalytic Cycles. *ACS Catal.* **2012**, *2*, 2787–2794.

(42) Abel, B. A.; Lidston, C. A. L.; Coates, G. W. Mechanism-inspired design of bifunctional catalysts for the alternating ring-opening copolymerization of epoxides and cyclic anhydrides. *J. Am. Chem. Soc.* **2019**, *141*, 12760–12769.

(43) Kim, H. K.; Yun, W. S.; Kim, M.-B.; Kim, J. Y.; Bae, Y.-S.; Lee, J.; Jeong, N. C. A Chemical route to activation of open metal sites in the copper-based metal-organic framework materials HKUST-1 and Cu-MOF-2. *J. Am. Chem. Soc.* **2015**, *137*, 10009–10015.

(44) Wade, C. R.; Dincă, M. Investigation of the Synthesis, Activation, and Isothermic Heats of CO₂ Adsorption of the Isostructural Series of Metal-Organic Frameworks M₃(BTC)₂ (M = Cr, Fe, Ni, Cu, Mo, Ru). *Dalton Trans.* **2012**, *41*, 7931–7938.

(45) Crispin, X.; Geskin, V.; Crispin, A.; Cornil, J.; Lazzaroni, R.; Salaneck, W. R.; Brédas, J.-L. Characterization of the interface dipole at organic/metal interfaces. *J. Am. Chem. Soc.* **2002**, *124*, 8131–8141.

(46) Hu, Z.; Zhong, Z.; Zhang, K.; Hu, Z.; Song, C.; Huang, F.; Peng, J.; Wang, J.; Cao, Y. Dipole formation at organic/metal interfaces with pre-deposited and post-deposited metal. *NPG Asia Mater.* **2017**, *9*, No. e379.

(47) Herges, R.; Geuenich, D. Delocalization of electrons in molecules. *J. Phys. Chem. A* **2001**, *105*, 3214–3220.

(48) Lam, M. K.; Lee, K. T.; Mohamed, A. R. Homogeneous, heterogeneous and enzymatic catalysis for transesterification of high free fatty acid oil (waste cooking oil) to biodiesel: A review. *Biotechnol. Adv.* **2010**, *28*, 500–518.

(49) You, Y.-D.; Shie, J.-L.; Chang, C.-Y.; Huang, S.-H.; Pai, C.-Y.; Yu, Y.-H.; Chang, C. H. Economic Cost Analysis of Biodiesel Production: Case in Soybean Oil. *Energ. Fuel.* **2008**, *22*, 182–189.

(50) DeSantis, D.; Mason, J. A.; James, B. D.; Houchins, C.; Long, J. R.; Veenstra, M. Techno-economic Analysis of Metal-Organic Frameworks for Hydrogen and Natural Gas Storage. *Energ. Fuel.* **2017**, *31*, 2024–2032.

(51) Nur Sulihatimsyila, A. W.; Lau, H. L. N.; Nabilah, K. M.; Nur Azreena, I. Refining process for production of refined palm-pressed fibre oil. *Ind. Crop. Prod.* **2019**, *129*, 488–494.

(52) Akusu, M. O.; Achinewhu, S. C.; Mitchell, J. Quality attributes and storage stability of locally and mechanically extracted crude palm oils in selected communities in Rivers and Bayelsa States, Nigeria. *Plant Foods Hum. Nutr.* **2000**, *55*, 119–126.

(53) Ong, L. K.; Effendi, C.; Kurniawan, A.; Lin, C. X.; Zhao, X. S.; Ismadji, S. Optimization of catalyst-free production of biodiesel from *Ceiba pentandra* (kapok) oil with high free fatty acid contents. *Energy* **2013**, *57*, 615–623.

(54) Gunawan, F.; Kurniawan, A.; Gunawan, I.; Ju, Y.-H.; Ayucitra, A.; Soetaredjo, F. E.; Ismadji, S. Synthesis of biodiesel from vegetable oils wastewater sludge by *in-situ* subcritical methanol transesterification: Process evaluation and optimization. *Biomass Bioenergy* **2014**, *69*, 28–38.